THE AMERICAN SOCIETY OF MECHANICAL ENGINEERS
345 E. 47th St., New York, N.Y. 10017

97-GT-187

DYNAMIC BEHAVIOR OF GEARED ROTORS

T. N. Shiau
National Chung Cheng University
Chia-Yi, Taiwan
J S Rao
Indian Institute of Technology
New Delhi, India

J. R. Chang
and
Siu-Tong Choi
National Cheng Kung University
Tainan, Taiwan

ABSTRACT

This paper is concerned with the dynamic behavior of geared rotor systems supported by squeeze film dampers, wherein coupled bending torsion vibrations occur. Considering the imbalance forces and gravity, it is shown that geared rotors exhibit chaotic behavior due to non linearity of damper forces. The route to chaos in such systems is established. In geared rotor systems, it is shown that torsional excitation can induce lateral vibrations. It is shown that squeeze film dampers can suppress large amplitudes of whirl arising out of torsional excitation.

INTRODUCTION

Determination of lateral and torsional frequencies of rotor systems is an important factor in the design of high speed rotor systems. Considerable amount of work has been reported in this direction, and reference may be made to Rao (1996).

When the drive system incorporates gear transmission units, the lateral and torsional modes get coupled. Lund (1978) considered such coupling in the torsional-lateral vibrations in a geared system of rotors. Shiau et al (1994) used a hybrid method to study the dynamic characteristics of geared rotor systems. Rao, Chang and Shiau (1995) developed a general finite element model to determine the coupled bending-torsion natural frequencies and mode shapes of geared rotors including the effect of pressure angle.

Squeeze film dampers are now commonly employed to suppress the lateral vibrations arising out of rotor imbalance. Mohan and Hahn (1974) considered the design of squeeze film damper supports for rigid rotors. Cookson and Kossa (1980) studied the effectiveness of squeeze film dampers for flexible rotors without a centralizing spring.

Hwang and Shiau (1991) applied Generalized Polynomial Expansion method to study the nonlinear effects of squeeze film forces on flexible rotors. They used Harmonic Balance Method associated with Time Collocation Method. Chen et. al. (1993) considered the application of squeeze film dampers to control lateral vibrations of a gear pair system. They reported one result with Poincare section from Direct Integration Method which indicated chaos in the system.

In geared rotor systems subjected to torsional excitation, the usual practice is to determine the torsional response and ignore the coupling of bending torsion vibrations, Rao et al (1980). This forms an important part of the geared rotors, particularly in the presence of short circuit excitation from the generator, see Rao (1996). Most important disturbances creating abnormal pulsating torques in a turbo-alternator system are: short circuit at generator terminals, faulty synchronizing, short circuit clearing, and line switching. Of these, sudden short circuit at generator terminals is considered to be the most unfavorable condition which sets up large torques in the rotor and induces severe stresses of the order of four to five times the normal values. Concordia (1956) gives details of these different electrical phenomena. Using a torsional analysis of a typical turbo-generator system, Rao (1992) has shown that the gear transmission unit can fail under high cycle fatigue due to an electrical short circuit torque.

In this paper, a simple gear pair system is first considered to obtain the coupled lateral-torsional response due to imbalance and gravity. Using FFT spectra as well as Poincare maps, the route to chaos is established. A geared rotor system is considered with short circuit excitation to determine the lateral response.

EQUATIONS OF MOTION

A typical geared rotor is shown in Fig. 1. Equations of motion of different elements are given below, see Rao, Chang and Shiau (1995).

Rigid Disk

The equations of motion of a rigid disk can be shown to be

$$[M^d]\{\ddot{q}^d\} + \Omega[G^d]\{\dot{q}^d\} = \{F_g^d\} \qquad (1)$$

where $\{q^d\}^T = \{\ V^d \ \ W^d \ \ B^d \ \ \Gamma^d \ \ \alpha^d \ \}$.

For the elements of the above matrices, see Rao, Chang and Shiau (1995)

Presented at the International Gas Turbine & Aeroengine Congress & Exhibition
Orlando, Florida — June 2–June 5, 1997
This paper has been accepted for publication in the Transactions of the ASME
Discussion of it will be accepted at ASME Headquarters until September 30, 1997

Shaft Element

The equations of motion of the shaft element can be shown as

$$[M^s]\{\ddot{q}^s\} + \Omega[G^s]\{\dot{q}^s\} + [K^s]\{q^s\} = \{F_s^s\} \quad (2)$$

where $\{q^s\}^T = \{\ V_1^s\ \ W_1^s\ \ B_1^s\ \ \Gamma_1^s\ \ a_1^s\ \ V_2^s\ \ W_2^s\ \ B_2^s\ \ \Gamma_2^s\ \ a_2^s\ \}$

and

$$[M^s] = [M_T^s] + [M_R^s] + [M_\theta^s]$$
$$[M_T^s] = [M_T^s]_0 + \Phi[M_T^s]_1 + \Phi^2[M_T^s]_2$$
$$[M_R^s] = [M_R^s]_0 + \Phi[M_R^s]_1 + \Phi^2[M_R^s]_2$$
$$[G^s] = [G^s]_0 + \Phi[G^s]_1 + \Phi^2[G^s]_2$$
$$[K^s] = [K^s]_0 + \Phi[K^s]_1 + [K_\theta^s]$$

For the elements of the above matrices, see Rao, Chang and Shiau (1995)

Axial Torque (Incremental Stiffness Matrix)

The effect of axial torque is considered by Zorzi and Nelson (1980) which gives rise to an incremental stiffness matrix. Rao, Chang and Shiau derived this incremental stiffness matrix for a Timoshenko shaft element.

Gear Pair

For the gear pair, we can obtain

$$\begin{bmatrix} [M_1^g] & \\ & [M_2^g] \end{bmatrix}\{\ddot{q}^g\} + \Omega_1 \begin{bmatrix} [G_1^g] & \\ & \frac{\Omega_2}{\Omega_1}[G_2^g] \end{bmatrix}\{\dot{q}^g\} - k_h \begin{bmatrix} [S_1] \\ [S_2] \end{bmatrix}\{q^g\} = \{F_s^g\} \quad (3)$$

where

$$[M_1^g] = [M_1^d] \text{ and } [G_1^g] = [G_1^d]$$
$$\{q^g\}^T = \{\ V_1^g\ \ W_1^g\ \ B_1^g\ \ \Gamma_1^g\ \ a_1^g\ \ V_2^g\ \ W_2^g\ \ B_2^g\ \ \Gamma_2^g\ \ a_2^g\ \}$$

and the elements of the remaining matrices can be taken from Rao, Chang and Shiau (1995)

Hydrodynamic Bearing

For a hydrodynamic bearing we have

$$\begin{bmatrix} c_{yy} & c_{yz} \\ c_{zy} & c_{zz} \end{bmatrix}\begin{Bmatrix} \dot{V}^b \\ \dot{W}^b \end{Bmatrix} + \begin{bmatrix} k_{yy} & k_{yz} \\ k_{zy} & k_{zz} \end{bmatrix}\begin{Bmatrix} V^b \\ W^b \end{Bmatrix} = \{F_s^b\} \quad (4)$$

Squeeze Film Damper Element

The damper forces are considered to be nonlinear. Neglecting fluid inertia and air entrainment effects, the radial and tangential components of the film forces using short bearing theory from Reynolds equation are, see Mohan and Hahn (1974)

$$F_r = -\frac{\mu R L^3}{c_r^2}\left(\varepsilon\dot{\phi}A^{11} + \dot{\varepsilon}A^{02}\right)$$
$$F_\phi = -\frac{\mu R L^3}{c_r^2}\left(\varepsilon\dot{\phi}A^{20} + \dot{\varepsilon}A^{11}\right) \quad (5)$$
$$A^{ij} = \int_{\phi_s+\pi}^{\phi_s+2\pi} \frac{\sin^i\theta\cos^j\theta}{(1-\varepsilon\cos\theta)^3}d\theta;\ \phi_s = \tan^{-1}\frac{\dot{\varepsilon}}{-\varepsilon\dot{\phi}}$$

The horizontal and vertical components of these forces are

$$F_V = \left(F_r V - F_\phi W\right) \div \sqrt{V^2+W^2}$$
$$F_W = \left(F_r W + F_\phi V\right) \div \sqrt{V^2+W^2} \quad (6)$$

SYSTEM EQUATIONS

The system equations can be written as

$$[M]\{\ddot{q}\} + [\Omega_1[G] + [C]]\{\dot{q}\} + ([K] - [K_T])\{q\} = \{F\} \quad (7)$$

where the force vector consists of imbalance forces, gravity, short circuit torque and squeeze film damper forces. Two specific examples are considered 1. A gear pair on squeeze film damper supports and 2. A geared turbo generator set.

GEAR PAIR ON SQUEEZE FILM DAMPER SUPPORTS

A simple gear pair mounted on squeeze film damper supports is considered here. The equations of motion can be shown to be

$$[M]\{\ddot{q}\} + (c_h[S_h] + [C_c])\{\dot{q}\} + (k_h[S_h] + [K_c])\{q\} = \{Q\} \quad (8)$$

where $\{q\} = \{\ V_1\ \ W_1\ \ a_1\ \ V_2\ \ W_2\ \ a_2\ \}^T$

$$[S_h] = \begin{bmatrix} S^2 & SC & r_1S & -S^2 & -SC & r_2S \\ SC & C^2 & r_1C & -SC & -C^2 & r_2C \\ r_1S & r_1C & r_1^2 & -r_1S & -r_1C & r_1r_2 \\ -S^2 & -SC & -r_1S & S^2 & SC & -r_2S \\ -SC & -C^2 & -r_1C & SC & C^2 & -r_2C \\ -r_2S & r_2C & r_1r_2 & -r_2S & r_2C & r_2^2 \end{bmatrix}$$

$$\{Q\} = \begin{Bmatrix} F_{V1} + M_1e_1\Omega_1^2\cos(\Omega_1 t + \psi_1) \\ F_{W1} + M_1e_1\Omega_1^2\sin(\Omega_1 t + \psi_1) - M_1 g \\ 0 \\ F_{V2} + M_2e_2\Omega_2^2\cos(\Omega_2 t + \psi_2) \\ F_{W2} + M_2e_2\Omega_2^2\sin(\Omega_2 t + \psi_2) - M_2 g \\ 0 \end{Bmatrix}$$

and non zero elements of $[M]$, $[C_c]$ and $[K_c]$ are

$$M_{11} = M_{22} = M_1, M_{44} = M_{55} = M_2, M_{33} = I_{p1} \text{ and } M_{66} = I_{p2}$$
$$C_{c11} = C_{c22} = C_1, C_{c44} = C_{c55} = C_2,$$
$$K_{c11} = K_{c22} = K_1, K_{c44} = K_{c55} = K_2,$$

In the above system of equations (8), the first two are divided by $M_1c_r\Omega_1^2$, the third one is divided by $I_{P1}\Omega_1^2$, the fourth and fifth by $M_2c_r\Omega_1^2$ and the sixth one by $I_{P2}\Omega_1^2$ to obtain the non dimensional form as

$$[I]\{\overline{q}''\} + \left(\frac{2\zeta_s}{\Omega_r}\left[\overline{S}_h\right] + \frac{2\zeta}{\Omega_r}\left[\overline{C}_c\right]\right)\{\overline{q}'\} + \left(\frac{\zeta_s}{\Omega_r^2}\left[\overline{S}_h\right] + \frac{1}{\Omega_r^2}\left[\overline{K}_c\right]\right)\{\overline{q}\} = \{\overline{Q}\} \quad (9)$$

where

$$\{\overline{q}\} = \{\ v_1\ \ w_1\ \ a_1\ \ v_2\ \ w_2\ \ a_2\ \}^T$$

$$\{\overline{Q}\} = \begin{Bmatrix} \frac{S_0}{\Omega_r}f_{v1} + U_1\cos(\tau + \psi_1) \\ \frac{S_0}{\Omega_r}f_{w1} + U_1\sin(\tau + \psi_1) - \frac{W_1}{\Omega_1^2} \\ 0 \\ \frac{S_0}{\eta_M\Omega_r}f_{v2} + \frac{U_2}{\eta_1^2}\cos\left(-\frac{\tau}{\eta_r} + \psi_2\right) \\ \frac{S_0}{\eta_M\Omega_r}f_{w2} + \frac{U_2}{\eta_1^2}\sin\left(-\frac{\tau}{\eta_r} + \psi_2\right) - \frac{W_2}{\Omega_1^2} \\ 0 \end{Bmatrix}$$

$$f_v = \left(f_r v - f_\phi w\right) \div \sqrt{v^2+w^2} \qquad f_w = \left(f_r w + f_\phi v\right) \div \sqrt{v^2+w^2}$$
$$f_r = -\left(\varepsilon\phi' A^{11} + \varepsilon' A^{02}\right) \qquad f_\phi = -\left(\varepsilon\phi' A^{20} + \varepsilon' A^{11}\right)$$
$$\overline{C}_{c11} = \overline{C}_{c22} = 1,\ \overline{C}_{c44} = \overline{C}_{c55} = \frac{\eta_c}{\eta_M} \quad \text{rest } \overline{C} = 0$$
$$\overline{K}_{c11} = \overline{K}_{c22} = 1,\ \overline{K}_{c44} = \overline{K}_{c55} = \frac{\eta_c}{\eta_M} \quad \text{rest } \overline{K} = 0$$

$$\left[\overline{S}_h\right] = \begin{bmatrix} S^2 & SC & \frac{S}{\zeta_c} & -S^2 & -SC & \frac{\eta_r S}{\zeta_c} \\ SC & C^2 & \frac{C}{\zeta_c} & -SC & -C^2 & \frac{\eta_r C}{\zeta_c} \\ \xi_1\xi_c S & \xi_1\xi_c C & \xi_1 & -\xi_1\xi_c S & -\xi_1\xi_c C & \xi_1\eta_r \\ \frac{-S^2}{\eta_M} & \frac{-SC}{\eta_M} & \frac{-S}{\eta_M\zeta_c} & \frac{S^2}{\eta_M} & \frac{SC}{\eta_M} & \frac{-\eta_r S}{\eta_M\zeta_c} \\ \frac{-SC}{\eta_M} & \frac{-C^2}{\eta_M} & \frac{-C}{\eta_M\zeta_c} & \frac{SC}{\eta_M} & \frac{C^2}{\eta_M} & \frac{-\eta_r C}{\eta_M\zeta_c} \\ \frac{\xi_1\zeta_c\eta_r S}{\eta_I} & \frac{\xi_1\zeta_c\eta_r C}{\eta_I} & \frac{\xi_1\eta_r}{\eta_I} & \frac{-\xi_1\zeta_c\eta_r S}{\eta_I} & \frac{-\xi_1\zeta_c\eta_r C}{\eta_I} & \frac{\xi_1\eta_r^2}{\eta_I} \end{bmatrix}$$

A computer program using Newmark's (1959) method is developed to determine the response of the above system of equations (9). Harmonic Balance method associated with Time Collocation is used for a typical case, only to verify the results obtained from Newmark's procedure. The gear pair chosen has the following data, $\xi_1 = 2, \xi_c = 10^{-5}, \eta_M, \eta_C, \eta_K, \eta_r, \eta_I, \xi_K = 1$, $\phi_p = 22.5°, \zeta_h = \zeta = 0.0005, S_D = 0.03, W_g = 0.1, \psi_1 = \psi_2 = 0$

The critical speeds due to synchronous excitation occur at Ω_r equal to 0 (rigid body torsional), 0.79 (coupled), 1.0, 1.0, 1.0 (lateral) and 2.52 (coupled). For an imbalance $U_1 = U_2 = 0.045$, $\Omega_r = 1.89$ with periodic solutions, results from both Newmark and Harmonic Balance methods are given in Fig. 2, which show good agreement. RK-5 solution is also tried, which gave similar results, however, it consumed considerably larger computer time and therefore has been dropped in favor of Newmark's method.

Effect of Imbalance

For the gear pair under consideration, the response obtained by Newmark's method is reported here. In all the cases, the initial conditions are kept the same, viz., zero for both the response and velocities. After reaching the steady state regime in time domain, 100 consecutive one-per-rotation speed marks, which appear on the response, are recorded. For periodic response all these marks appear at a constant position for any number of rotations. For a steady synchronous response, there will be only one mark. If the response is half synchronous, there will be two marks, etc. If the response is chaotic, multiple marks result from these consecutive one hundred positions, also see Goldman and Muszynska (1994) and Ehrich (1995). These positions for both the vertical and horizontal response of the system are given as bifurcation maps in Figs. 3 and 4 for an imbalance of $U_1 = U_2 = 0.045$, Figs. 5 and 6 for $U_1 = U_2 = 0.1$ and Figs. 7 and 8 for $U_1 = U_2 = 0.45$.

It can be seen from Figs. 3 and 4 that the response is almost periodic except for a very narrow region near the second coupled mode $\Omega_r = 2.52$. In Figs. 5 and 6 the chaotic region is still around the second coupled mode but a little wider than in Figs. 3 and 4. With a further larger imbalance, $U_1 = U_2 = 0.45$, the influence on the chaotic range becomes significant as shown in Figs. 7 and 8. Here, the chaotic region is divided into two wider parts on both sides of the second coupled mode region. The response is periodic for $\Omega_r < 1.75$. Beyond this region, the response becomes chaotic with intermittent zones of periodic solutions. It is also clear from these figures that the response is periodic around all the critical speeds, 0.79 (coupled), 1.0, 1.0, 1.0 (lateral) and 2.52 (coupled).

Typical responses obtained by Newmark's direct integration method for $\Omega_r = 1.83, 1.85, 1.867$ and 1.8 are given in Figs. 9 to 12 respectively, where (a) shows the orbital response of the driving gear, (b) that of driven gear, (c) spectra of the semi-major axis of the driving gear and (d) gives the Poincare map for response of the driving gear in horizontal direction. It can be seen from Fig. 9 that the response has no sub harmonic for $\Omega_r = 1.83$, however, there are super harmonics possible.

Just by increasing Ω_r from 1.83 to 1.85, the result in Fig. 10 shows that the response becomes quasi-periodic, see Thomson and Stewart (1986). The quasi-periodic solutions result in closed orbits on Poincare map as shown in Fig. 10d. It can also be seen from Fig. 10c, the frequency spectrum contains two fundamental components $p_1 = \Omega_1$ and $p_2 = 0.627\Omega_1$. These *incommensurate* frequencies are related by an irrational factor. The remaining are combinations of the fundamental components, given by

$0.119\Omega_1 = 2p_1 - 3p_2$, $0.254\Omega_1 = 2p_2 - p_1$,
$0.373\Omega_1 = p_1 - p_2$, $0.492\Omega_1 = 3p_1 - 4p_2$
$0.508\Omega_1 = 4p_2 - 2p_1$, $0.746\Omega_1 = 2p_1 - 2p_2$
$0.881\Omega_1 = 3p_2 - 2p_1$, etc.

Since there are two fundamental components and that it is difficult to guess both of them, e.g., $p_2 = 0.627\Omega_1$ in this case, it can be clearly observed that Harmonic Balance method is not applicable to determine the system response. The factor 0.627 is different for different spin speeds, e.g., for $\Omega_r = 1.86$, it is 0.631.

By increasing the frequency ratio further to $\Omega_r = 1.867$, the quasi-periodic motion of Fig. 10 tends to become chaotic as shown in Fig. 11. This is typically the transition observed from quasi-periodic motion to chaotic motion as reported by Singh et. al. (1992). For $\Omega_r = 1.89$, the system experiences a clear chaos as can be seen in Fig. 12.

In addition, the jump phenomena is also found in Figs. 7 and 8 in two regions at $\Omega_r = 1.33 - 1.34$ and $1.79 - 1.80$. The orbital response at $\Omega_r = 1.3338$ & 1.3339 is shown in Fig. 13. It shows that the driving gear orbits at these two close spin speed ratios are quite different though the driven gear orbits are very close.

Effect of Gravity

For the gear pair data chosen earlier, the bifurcation maps obtained with $W_g = 0.0$, are found to be similar to those of Figs. 7 and 8 with 0.45 imbalance. However, the larger the gravity say, $W_g = 1$, at $\Omega_r = 1.89$, the larger the offset of both gear centers as shown in Fig. 14. Comparing Figs. 12c and 14c, we find that the broad band spectrum with $W_g = 0.1$ now has many discrete peaks at zero frequency and multiples of spin speed. Further, the Poincare map containing many points in Fig. 12d now contains only one mark as shown in Fig. 14d. Therefore gravity has a tendency to remove chaos in the system.

Effect of Squeeze Film Damper

For $S_D = 0.1$, Figs. 15 and 16 give the bifurcation maps which show that the response is periodic for $\Omega_r < 2.13$ and that the chaotic regime has intermittent zones of periodic response. Comparing these figures with Figs. 7 and 8, we find that major range of chaos for $S_D = 0.03$ is 1.8 to 2.38 and above 2.64 and for $S_D = 0.1$, it is 2.13 to 2.3 and above 2.5.

At $\Omega_r = 1.89$, the orbital responses of both gears, the associated spectra and Poincare maps are given in Figs. 17 and 18 for $S_D = 0.05$ and 0.1 respectively. We find the chaos of Fig. 12 becomes quasi-periodic in Fig. 17 and as damping becomes larger the spectrum in Fig. 18 shows periodic-one solution.

For the system under consideration, the resonant response at $\Omega_r = 1$ obtained without the squeeze film dampers, $S_D = 0$, is given in Fig. 19. The response is 470 times that of the clearance. To control these large whirl amplitudes, we can use a squeeze film damper in the supports. For a value of $S_D = 0.03$ of the squeeze film damper, the response is predominantly suppressed and contained within the clearance as shown in Fig. 20.

Effect of Mesh Stiffness

Keeping all the parameters as considered above, when the mesh stiffness is changed the natural frequencies change, e.g., when $\xi_K = 0.1$ the critical speeds are Ω_r= 0, 0.55 (coupled) 1.0, 1.0, 1.0 (lateral) and 1.13 (coupled). Chaotic response is found in this case also around the second coupled mode as in the previous cases with intermittent zones of periodic responses.

Effect of Imbalance Phase Angle

Keeping $\psi_1 = 0$, increasing ψ_2 makes the chaos disappear, e.g., when $\psi_2 = 45°$ quasi-periodic response was observed with two or more incommensurate frequencies. For $\psi_2 = 90°$ seven fold loop motions are observed as shown in Figs. 21a and 21b, though the loops shown are very close in Fig. 21b. The FFT spectrum has peaks at zero frequency and the integer multiples of 1/7 sub-harmonic frequency as shown in Fig. 21c. Seven points are found on the Poincare map of Fig. 21d. It shows that the steady state solution for this case is periodic and classified to be period-seven. When $\psi_2 = 180°$ the results are shown in Fig. 22. It is interesting to see that sevenfold loop orbits occur again, though the orbit of the driving gear is almost like a circle.

GEARED TURBO GENERATOR SET

Referring to Fig. 1 the following data is chosen. M_{10}=7.45, M_2=525.7, M_3=116.04, M_7=5.0 and M_6=726.4 kg; I_{T10}=0.0745, I_{T2}=16.1, I_{T3}=3.115, I_{T7}=0.002 and I_{T6}=56.95 kgm^2; I_{P10}=0.149, I_{P2}=32.2, I_{P3}=6.23, I_{P7}=0.004 and I_{P6}=113.9 kgm^2.

The pinion has 23 teeth with r_7=0.03567m while the gear has 328 teeth with r_6=0.5086m, $k_h = 10^8$ N/m and $\phi_p = 22.5°$. Shaft lengths between nodes are taken as: l_{12}=0.1, l_{23}=4.24, l_{34}=1.16, l_{45}=l_{56}=0.15, l_{78}=0.3, l_{89}=0.05, $l_{9,10}$=4.95 and $l_{10,11}$=0.1 m, radius between nodes 1 and 3 = 0.15 m, between nodes 3 and 6 = 0.11m and for turbine shaft = 0.075 m. Young's modulus=207 GPa, Shear modulus = 79.5 GPa and density = 7800 Kg/m^3.

Bearings 1 and 2 have $k_{yy} = 1.839 \times 10^8$, $k_{zz} = 2.004 \times 10^8$ and bearings 3 and 4 $k_{yy} = 1.010 \times 10^7$,$k_{zz} = 4.160 \times 10^7$ N/m. Damping in all bearings = 3000 Ns/m. Nominal torque T_n = 318.31 Nm. The short circuiting torque, see Rao (1992), is

$$T = T_n m_a e^{-\alpha t} \sin \omega t + T_n m_s e^{-\beta t} \sin 2\omega t \qquad (10)$$

where $m_a = 12.353$, $m_s = 0.5$, $\alpha = 33.97$ and $\beta = 5.45$.

The coupled natural frequencies of the system for Ω_1 = 1500 rpm (157.08 rad/s) are 73.1, 77.2, 108.5, 116.0, 150.5, 236.8, 313.5, 319.6, 353.5, 362.9, 371.9, 396.6 and 466.2 rad/s.

Since the rotational speed is close to the coupled natural frequency 150.5 rad/s, the predominant frequency components of the lateral and torsional response will occur at this mode shape. This mode shape is shown in Fig. 23.

An uncentralized spring configuration for the damper is chosen with R=50.8 and L=25.4 mm. Three arrangements are chosen: I. μ=0.015016 Ns/m^2, c_r =152.4 microns, II. μ=0.015016 Ns/m^2, c_r =304.8 microns and III. μ=0.030032 Ns/m^2, c_r =152.4 microns. The shaft torques without damper for sections 4-5, 5-6 near the gear and 7-8 near the pinion are shown in Fig. 24a. The corresponding torques for case I-5 (Squeeze Film Damper I at location 5) are shown in Fig. 25a. The torque value initially is larger than the undamped case, however, it decays faster because of squeeze film damper (the difference in torque values is very small as the amplitude at node 5 in Fig. 23 is very small). For case I-9, the corresponding values given in Fig. 26a show that the damper location 9 is far more effective in decreasing the torque values in a shorter time. This can be confirmed from Fig. 27a with two dampers I-5+9 (located at 5 and 9) since the torque response is almost same as in case I-9.

The lateral response of both the gear and pinion is given in Fig. 24b for the undamped case. The pinion response is nearly 8 times that of the gear. With I-5 arrangement, the response given in Fig. 25b, shows it has practically no effect on the response. However, with the damper located at station 9 (I-9), it has a significant influence in reducing the pinion response by nearly 2.5 times as can be seen from Fig. 26b. As in the case of shaft torques, the arrangement I-5+9 gives a response shown in Fig. 27b, same as in Fig. 26b. Therefore, it can be deduced that the squeeze film damper should be located near the pinion experiencing maximum lateral response.

The undamped torsional response for both the pinion and gear is shown in Fig. 24c. The corresponding response for the case I-5 is given in Fig. 25c. The damper becomes effective when it is located at station 9 and for clarity only the pinion response is shown in Fig. 26c. As in the previous cases the response, though initially larger decays rapidly. The high frequency component is also clearly seen. Fig. 27c shows the response with I-5+9 arrangement.

The lateral response for case II-9 is shown in Fig. 28a. Compared to Fig. 26b (I-9), the response here is nearly 1.6 times larger for the pinion and almost the same for the gear. With a larger clearance, damping force decreases as can be seen from equation (5) and therefore, the effect of squeeze film damper is also decreased. Fig. 28b shows the results for case III-9, which has double the viscosity compared to I-9. The peak ampliyude is slightly lower in Fig. 28b and decreases faster than that in Fig. 26b. Fig. 29 shows the force transmitted by the damper at node 9 for case I-9. It can be seen that the transmitted force decreases rapidly because of the damping action.

CONCLUSIONS

Considering a simple gear pair system with nonlinear squeeze film damper supports, the response is shown to be periodic, quasi-periodic and transitional in nature before becoming chaotic. Under quasi-periodic conditions, the response typically contains two fundamental components and several combinations of these components. Through bifurcation diagrams, the chaotic

behavior of the system is discussed. It is shown that 1. The larger the imbalance, the wider the chaotic regime, 2. gravity suppresses chaos in the system, 3. increasing the damping coefficient can reduce the chaotic region, 4. irrespective of mesh stiffness values, chaos occurs around the second coupled mode and 5. in-phase unbalances give rise to chaos, as the relative phase angle increases, the response becomes quasi-periodic and with out-of-phase imbalances it is periodic. Coupled bending-torsion vibrations of a geared turbine are considered. The lateral response due to short circuit torque is determined and shown to be substantial. It is shown that squeeze film dampers can be used to suppress the lateral response arising from torsional excitation.

ACKNOWLEDGMENTS

The authors are very thankful to the National Science Council of Taiwan for the grant NSC 84-2212-E-194-001 and to provide a research chair to Professor J S Rao during 1994-96.

REFERENCES

Chen, Chin-Shong et. al., 1993, "Coupled Lateral-Torsional Vibration of A Gear Pair System Supported by A Squeeze Film Damper", *ASME Design Engineering Div.*, Vol. 54, p. 53

Concordia, C., 1956, *Synchronous Machine Theory and Performance*, John Wiley and Sons, New York

Cookson, R. A. and Kossa, S. S., 1980, "The Effectiveness of Squeeze Film Damper Bearings Supporting Flexible Rotors without a Centralizing Spring" *Intl. J Mech. Sci.*, Vol. 22, 313

Ehrich, F., 1995, "Nonlinear Phenomena in Dynamic Response of Rotors in Anisotropic Mounting Systems", ASME *Special 50th Anniversary Design Issue*, Vol. 117, p. 154

Goldman, P. and Muszynska, A., 1994, "Chaotic Behavior of Rotor/Stator Systems with Rubs", *ASME J of Engng. for Gas Turbines and Power*, Vol. 116, p. 692

Hwang, J. L. and Shiau, T. N., 1991, "An Application of the Generalized Polynomial Expansion Method to Nonlinear Rotor Bearing Systems", *ASME J Vib. and Acoust.*, Vol. 113, 299

Lund, J., 1978, "Critical Speed, Stability and Response of a Geared Train of Rotors", *J Mechanicol Design, Trans. ASME*, Vol. 100, p. 535

Mohan, S. and Hahn, E. J., 1974, "Design of Squeeze Film Damper Supports for Rigid Rotors", ASME *J of Engng. for Indus*, Vol. 96, No. 3, p. 976

Newmark, N. M., 1959, "A Method of Computation for Structural Dynamics", *Proc. ASCE*, Vol. 85 (EM3), p. 67

Rao, J. S., 1992, "Life Estimation of Gear Transmission Unit in a Turbine Generator Set due to Short Circuits", *Mechonism and Machine Theory*, Vol. 27, No. 3, p. 283

Rao, J. S., 1996, *Rotor Dynamics*, 3rd edition, New Age International, New Delhi, London

Rao, J. S., Chang, J. R. and Shiau, T. N., 1995 "Coupled Bending-Torsion Vibration of Geared Rotors", *ASME Design Engng Technical Confs*, DE-Vol. 84-2, Vol. 3 - Part B, p. 977

Rao, J. S., Chang, J. R. and Shiau, T. N., Lateral Response due to Torsional Excitation of Geared Rotors, submitted to *Mechanism and Machine Theory*

Rao, J. S., Rao, D. K. and Bhaskara Sarma, K. V., 1980, "The Transient Response of Turbo-Alternator Rotor Systems under Short Circuiting Conditions", *Proc. Vibrations of Rotating Machinery Conf.* Instn. of Mech. Engrs., p. 271

Shiau, T. N., Chou, Y. W., Chang, J. R. and Nelson, H. D., 1994, "A Study on the Dynamic Characteristics of Geared Rotor-Bearing System with Hybrid Method", *ASME 94-GT-355*

Singh, R. et. al. 1990, *Nonlinear Dynamic Analysis of Geared Systems*, NASA Contractor Report 4338

Thomson, J. M. T. and Stewart, H. B., 1986, *Nonlinear Dynamics and Chaos*, John Wiley.

Zorzi, E. S. and Nelson, H. D., 1980, The Dynamics of Rotor Bearing Systems with Axial Torque: A Finite Element Approach, *ASME J of Mech. Des.*, Vol. 102, 158

NOMENCLATURE

C_1, C_2	centralizing spring damping coefficients
C, S	$\cos\phi_p$, $\sin\phi_p$
c_h	gear mesh damping coefficient
c_r	radial clearance
c_{yy}, c_{zz}	direct damping coefficients
c_{yz}, c_{zy}	cross-coupled damping coefficients
e	eccentricity
F, f	sfd force, non dimensional sfd force
I_P	polar mass moment of inertia
K	centralizing spring stiffness
k_h	gear mesh stiffness
k_{yy}, k_{zz}	direct stiffness coefficients
k_{yz}, k_{zy}	cross-coupled stiffness coefficients
L	length of squeeze film damper
M	mass
R	journal radius
r	gear base circle radius
$[S_1], [S_2]$	gear mesh stiffness matrices
S_D	$\mu RL^3 + (M_1 c_r^3 \omega_1)$
$[S_h]$	gear mesh stiffness matrix
U, W_g	$e + c_r, g + \left(c_r \omega_1^2\right)$
V, W	lateral displacements in Y, Z directions
v, w	$V + c_r, W + c_r$
a	torsional displacement about X direction
α, β	saliency constants
B, Γ	angles of rotation about Y, Z directions
ε	$\sqrt{v^2 + w^2} + c_r$
$\dot{\phi}$	angular velocity of journal
ϕ_p	pressure angle
η_C, η_K, η_M	$C_2 + C_1$, $K_2 + K_1$, $M_2 + M_1$
η_I, η_r	$I_{P2} + I_{P1}$, $r_2 + r_1$
ξ_c, ξ_I, ξ_K	$c_r + r_1, M_1 r_1^2 + I_{P1}, k_h + K_1$
ζ, ζ_h	$C_1 + (2M_1\omega_1), C_h + (2M_1\omega_1)$
μ	viscosity of lubricant
ω_1	$\sqrt{K_1/M_1}$
Ω	rotational (spin) speed
Ω_r	Ω_1/ω_1
τ	$\Omega_1 t$
$'$	denotes differentiation with τ

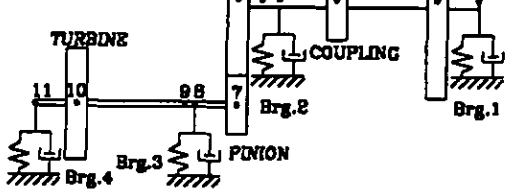

Fig.1 Geared turbo generator set

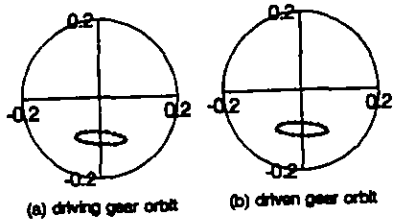

Fig.2 Comparison of results

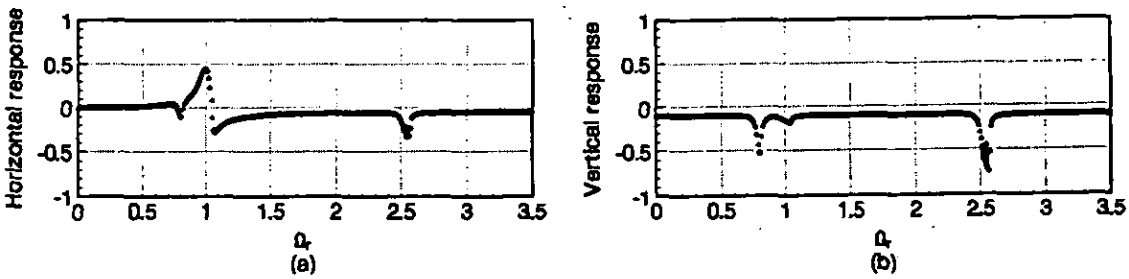

Fig.3 Bifurcation maps of driving gear response for $U_1 = U_2 = 0.045$

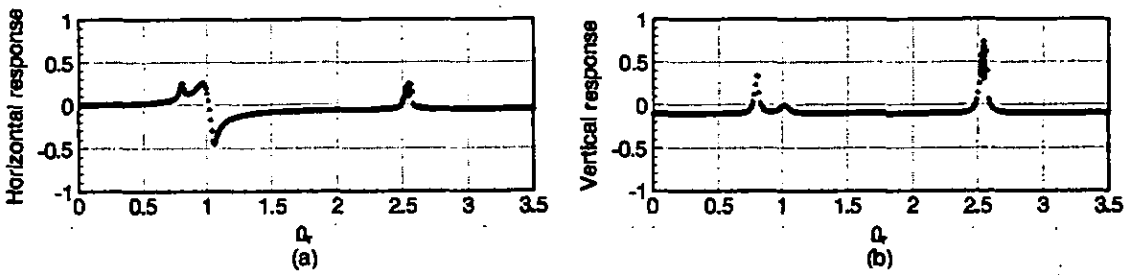

Fig.4 Bifurcation maps of driven gear response for $U_1 = U_2 = 0.045$

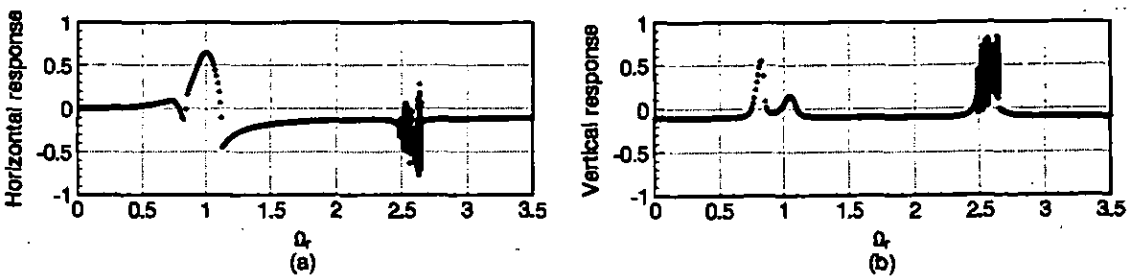

Fig.5 Bifurcation maps of driving gear response for $U_1 = U_2 = 0.1$

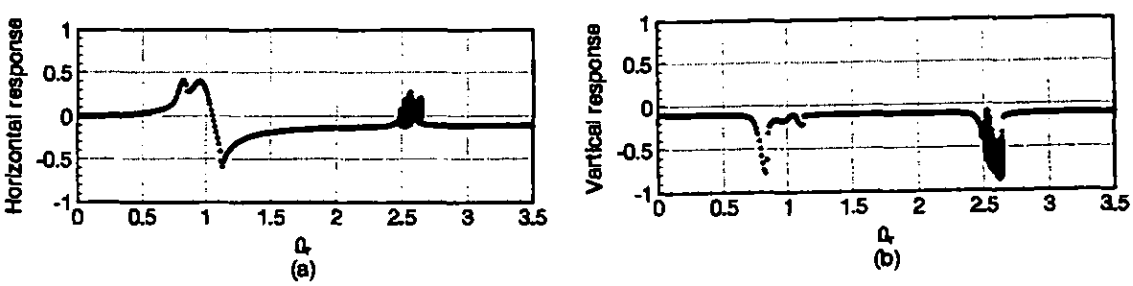

Fig.6 Bifurcation maps of driven gear response for $U_1 = U_2 = 0.1$

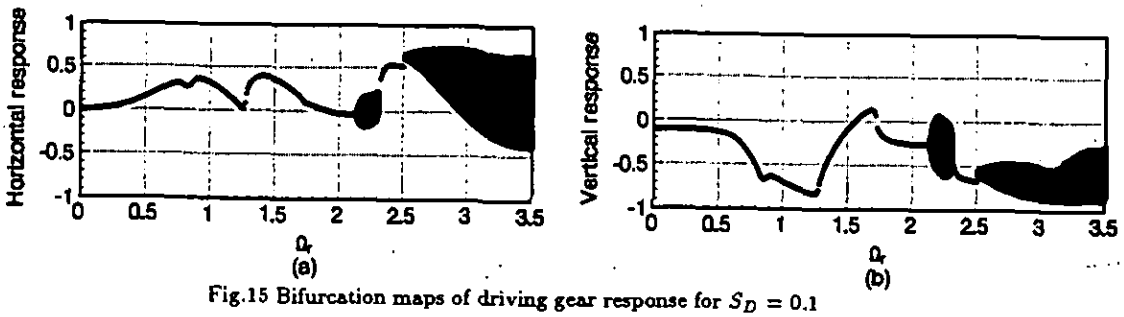

Fig.15 Bifurcation maps of driving gear response for $S_D = 0.1$

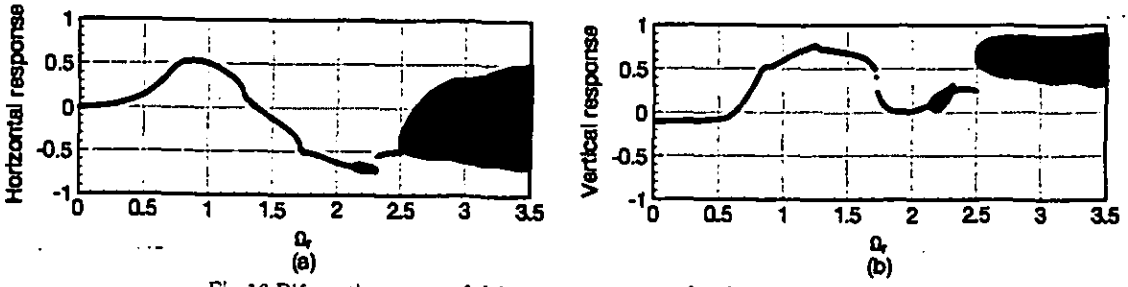

Fig.16 Bifurcation maps of driven gear response for $S_D = 0.1$

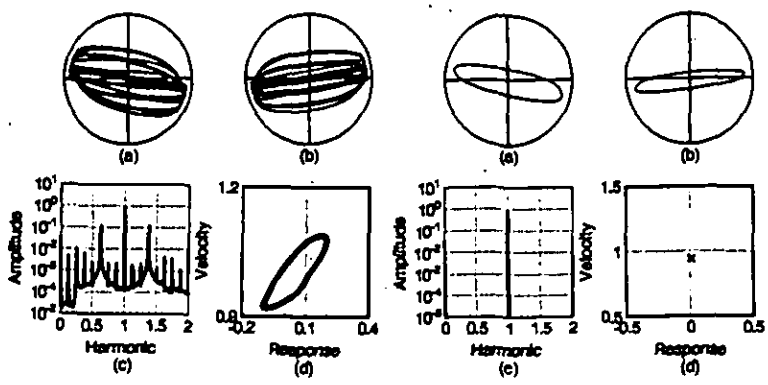

Fig.17 Response for $S_D = 0.05$

Fig.18 Response for $S_D = 0.1$

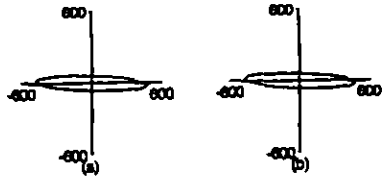

Fig.19 Response without squeeze film damper $\Omega_r = 1$

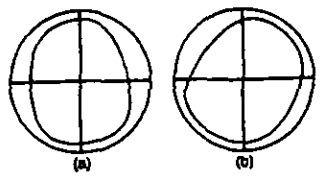

Fig.20 Response with squeeze film damper $S_D = 0.03$, $\Omega_r = 1$

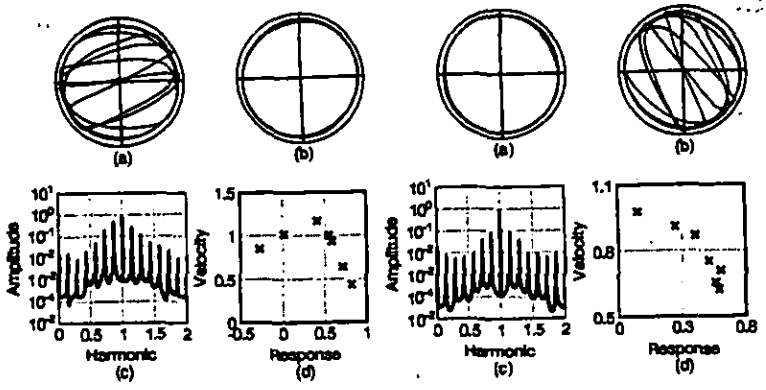

Fig.21 Response for $\psi_1 = 0°$, $\psi_2 = 90°$

Fig.22 Response for $\psi_1 = 0°$, $\psi_2 = 180°$

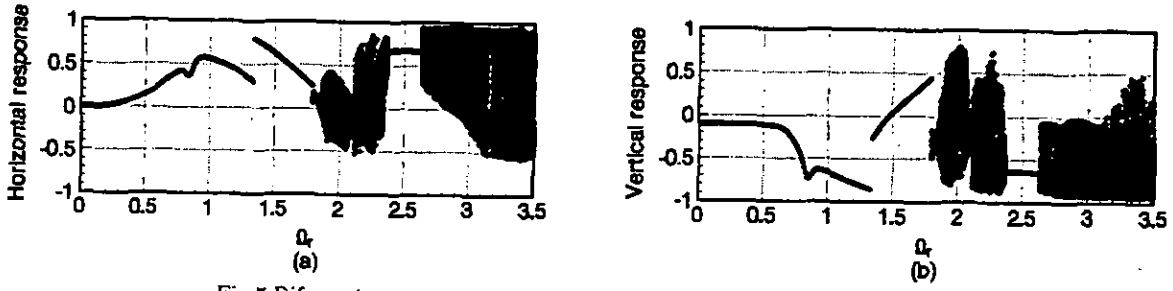

Fig.7 Bifurcation maps of driving gear response for $U_1 = U_2 = 0.45$

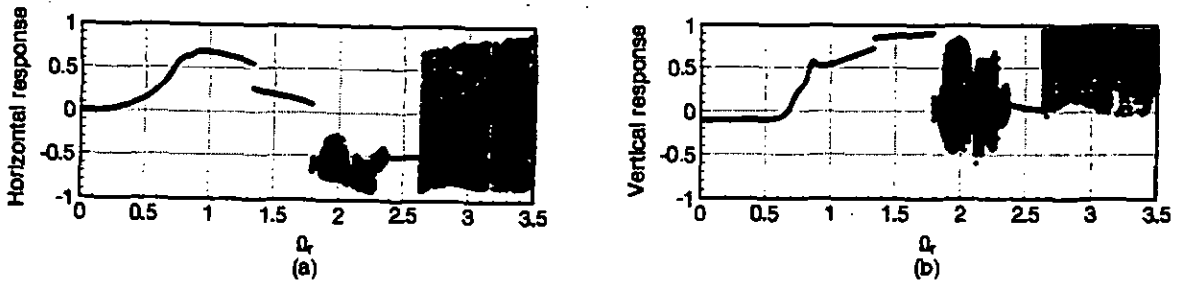

Fig.8 Bifurcation maps of driven gear response for $U_1 = U_2 = 0.45$

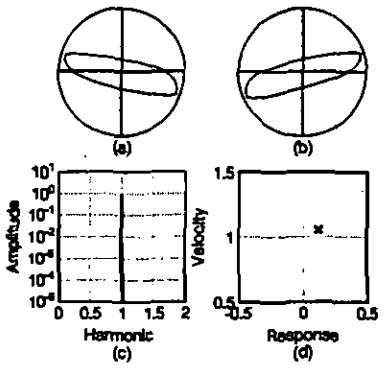

Fig.9 Response for $\Omega_r = 1.83$

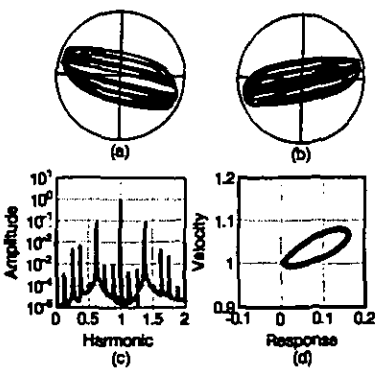

Fig.10 Response for $\Omega_r = 1.85$

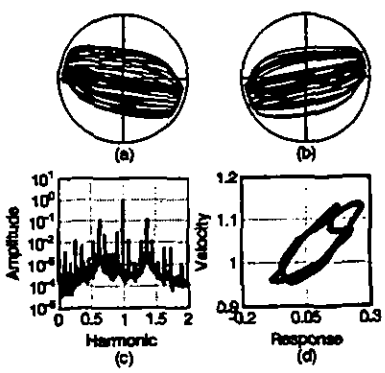

Fig.11 Response for $\Omega_r = 1.867$

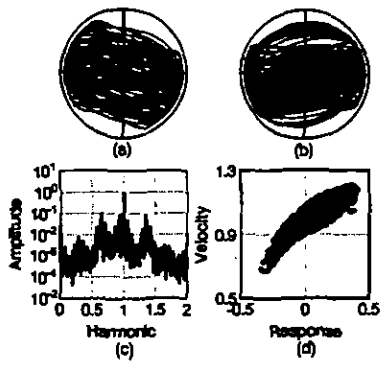

Fig.12 Response for $\Omega_r = 1.89$

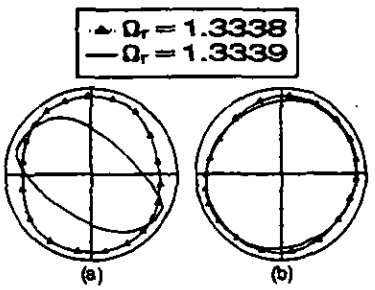

Fig.13 Orbital responses for $\Omega_r = 1.3338$ and 1.3339

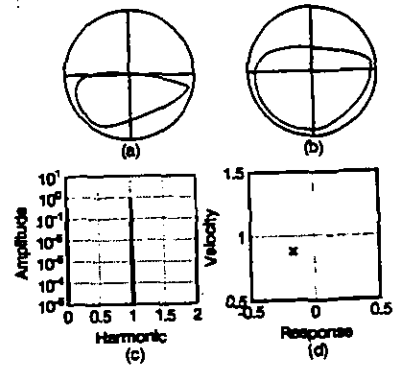

Fig.14 Response for $W_g = 1$

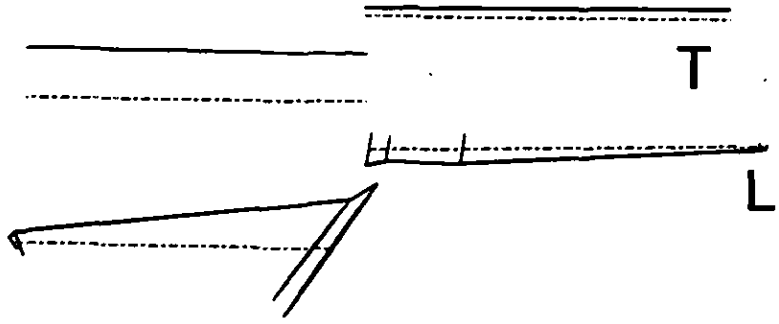

Fig.23 Mode shape of natural frequency 150.5rad/s at Ω_1 = 1500rpm

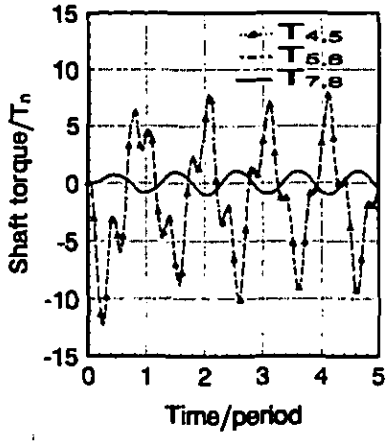

Fig.24a Shaft torques without SFD

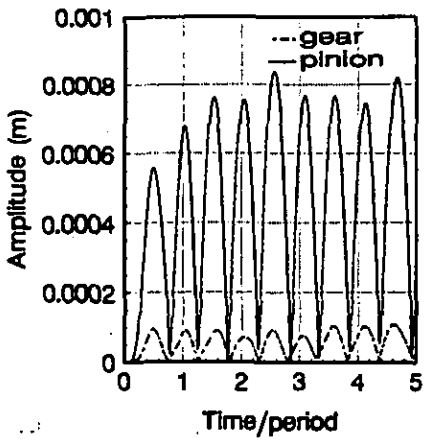

Fig.24b Lateral response without SFD

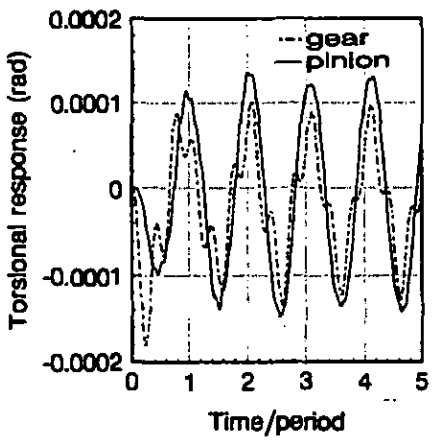

Fig.24c Torsional response without SFD

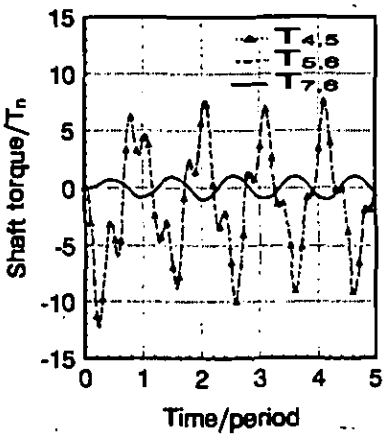

Fig.25a Shaft torques with SFD I-5

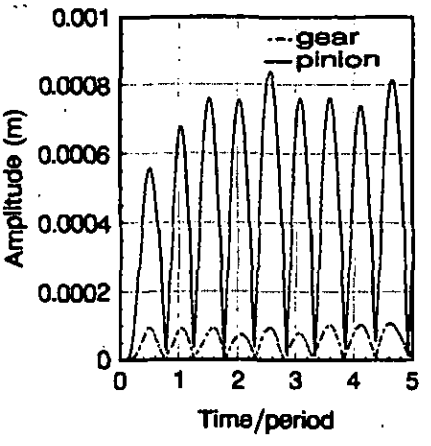

Fig.25b Lateral response with SFD I-5

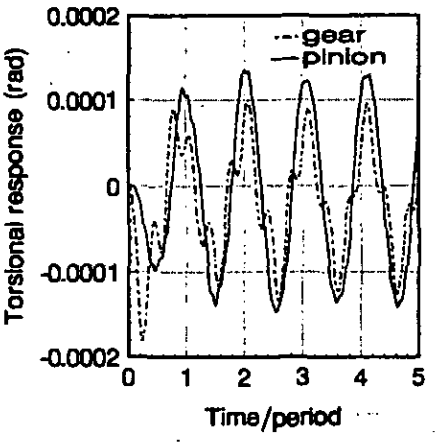

Fig.25c Torsional response with SFD I-5

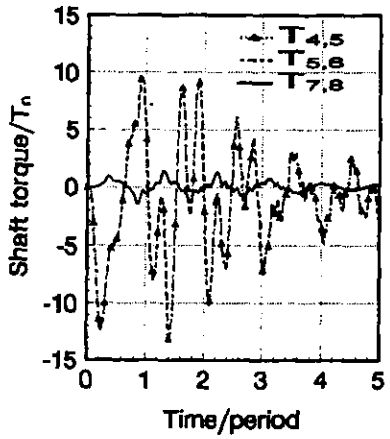

Fig.26a Shaft torques with SFD I-9

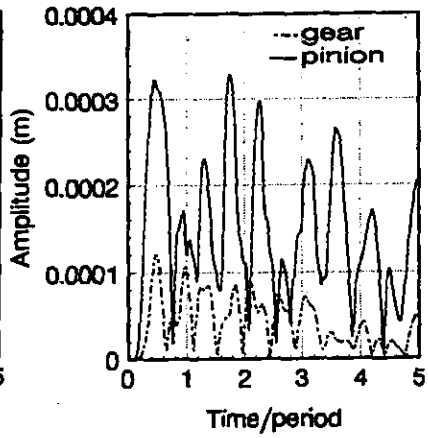

Fig.26b Lateral response with SFD I-9

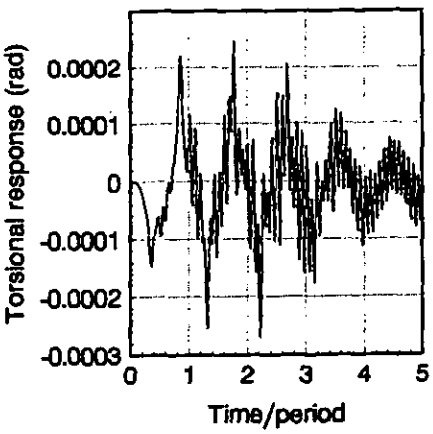

Fig.26c Torsional response of pinion with SFD I-9

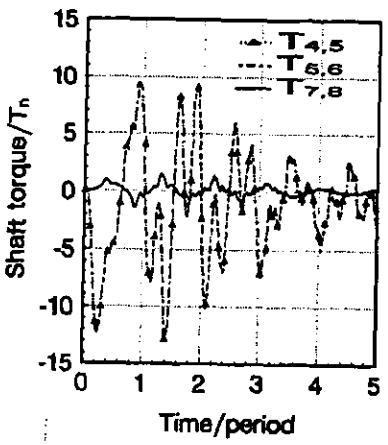

Fig.27a Shaft torques with SFD I-5+9

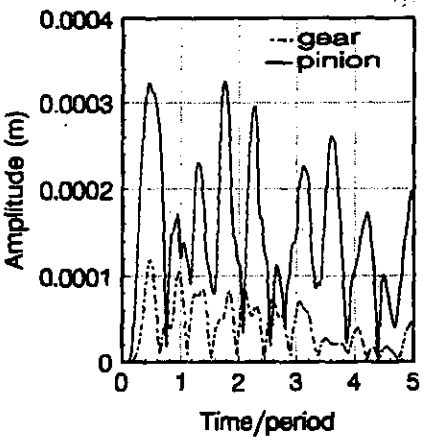

Fig.27b Lateral response with SFD I-5+9

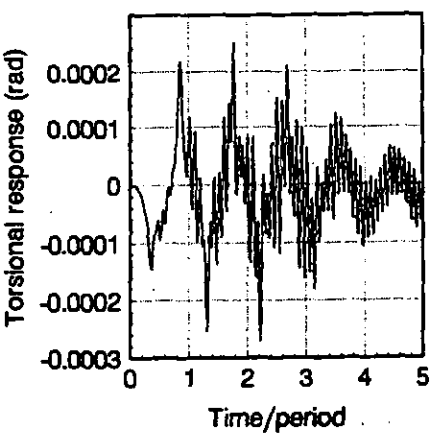

Fig.27c Torsional response of pinion with SFD I-5+9

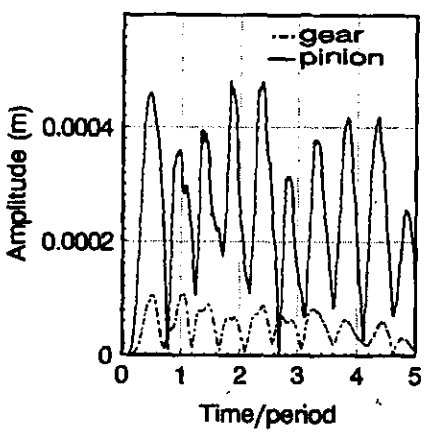

Fig.28a Lateral response with SFD II-9

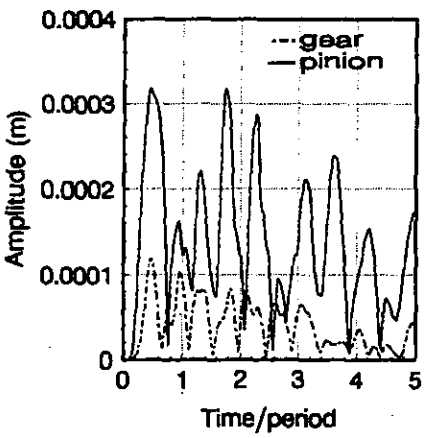

Fig.28b Lateral response with SFD III-9

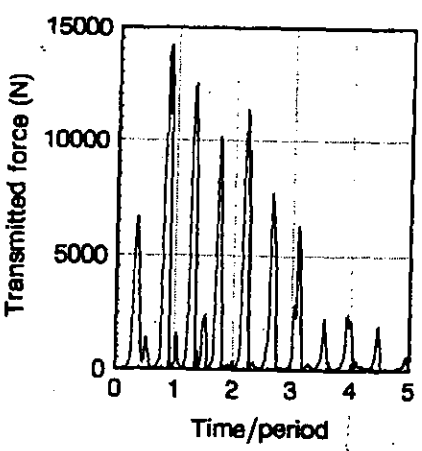

Fig.29 Transmitted force at node 9 with SFD I-9